



# Integrating Landsat pixel composites and change metrics with lidar plots to predictively map forest structure and aboveground biomass in Saskatchewan, Canada



Harold S.J. Zald<sup>a,\*</sup>, Michael A. Wulder<sup>b</sup>, Joanne C. White<sup>b</sup>, Thomas Hilker<sup>a</sup>, Txomin Hermosilla<sup>c</sup>,  
Geordie W. Hobart<sup>b</sup>, Nicholas C. Coops<sup>c</sup>

<sup>a</sup> Department of Forest Engineering Resources and Management, College of Forestry, Oregon State University, Corvallis, OR 97331, USA

<sup>b</sup> Pacific Forestry Centre, Canadian Forest Service, Natural Resources Canada, Victoria, British Columbia V8Z 1M5, Canada

<sup>c</sup> Integrated Remote Sensing Studio, Department of Forest Resources Management, University of British Columbia, Vancouver, British Columbia V6T 1Z4, Canada

## ARTICLE INFO

### Article history:

Received 9 July 2015

Received in revised form 2 December 2015

Accepted 20 January 2016

Available online xxxx

### Keywords:

Lidar

Landsat

Pixel composites

Change metrics

Random forest

Imputation

## ABSTRACT

Forest inventory and monitoring programs are needed to provide timely, spatially complete (i.e. mapped), and verifiable information to support forest management, policy formulation, and reporting obligations. Satellite images, in particular data from the Landsat Thematic Mapper and Enhanced Thematic Mapper (TM/ETM+) sensors, are often integrated with field plots from forest inventory programs, leveraging the complete spatial coverage of imagery with detailed ecological information from a sample of plots to spatially model forest conditions and resources. However, in remote and unmanaged areas such as Canada's northern forests, financial and logistic constraints can severely limit the availability of inventory plot data. Additionally, Landsat spectral information has known limitations for characterizing vertical vegetation structure and biomass; while clouds, snow, and short growing seasons can limit development of large area image mosaics that are spectrally and phenologically consistent across space and time. In this study we predict and map forest structure and aboveground biomass over 37 million ha of forestland in Saskatchewan, Canada. We utilize lidar plots—observations of forest structure collected from airborne discrete-return lidar transects acquired in 2010—as a surrogate for traditional field and photo plots. Mapped explanatory data included Tasseled Cap indices and multi-temporal change metrics derived from Landsat TM/ETM+ pixel-based image composites. Maps of forest structure and total aboveground biomass were created using a Random Forest (RF) implementation of Nearest Neighbor (NN) imputation. The imputation model had moderate to high plot-level accuracy across all forest attributes ( $R^2$  values of 0.42–0.69), as well as reasonable attribute predictions and error estimates (for example, canopy cover above 2 m on validation plots averaged 35.77%, with an RMSE of 13.45%, while unsystematic and systematic agreement coefficients ( $AC_{uns}$  and  $AC_{sys}$ ) had values of 0.63 and 0.97 respectively). Additionally, forest attributes displayed consistent trends in relation to the time since and magnitude of wildfires, indicating model predictions captured the dominant ecological patterns and processes in these forests. Acknowledging methodological and conceptual challenges based upon the use of lidar plots from transects, this study demonstrates that using lidar plots and pixel compositing in imputation mapping can provide forest inventory and monitoring information for regions lacking ongoing or up-to-date field data collection programs. Crown Copyright © 2016 Published by Elsevier Inc. This is an open access article under the CC BY-NC-ND license (<http://creativecommons.org/licenses/by-nc-nd/4.0/>).

## 1. Introduction

Forests cover approximately 31% of global land surface area (FAO, 2010), providing critical ecosystem services such as wood products, wildlife habitat, biodiversity, and regulation of the earth's biogeochemical cycles (Daily, 1997; Millennium Ecosystem Assessment, 2005). In Canada, forests cover over 400 million ha, representing more than 53% of Canada's land area and accounting for approximately 10% of global forest cover (Natural Resources Canada, 2014). Canada's forests make significant contributions to global bio-geochemical cycles and provide

\* Corresponding author at: 280 Peavy Hall, Oregon State University, Corvallis, OR 97331, USA.

E-mail addresses: [harold.zald@oregonstate.edu](mailto:harold.zald@oregonstate.edu) (H.S.J. Zald), [mike.wulder@canada.ca](mailto:mike.wulder@canada.ca) (M.A. Wulder), [joanne.white@canada.ca](mailto:joanne.white@canada.ca) (J.C. White), [thomas.hilker@oregonstate.edu](mailto:thomas.hilker@oregonstate.edu) (T. Hilker), [txomin.hermosilla@live.forestry.ubc.ca](mailto:txomin.hermosilla@live.forestry.ubc.ca) (T. Hermosilla), [geordie.hobart@canada.ca](mailto:geordie.hobart@canada.ca) (G.W. Hobart), [nicholas.coops@ubc.ca](mailto:nicholas.coops@ubc.ca) (N.C. Coops).

a wide array of other ecosystem services (Natural Resources Canada, 2014). Sustainable management and conservation of forests to maintain these services requires consideration of a wide array of ecological, economic, and societal values. To inform these needs, comprehensive inventory and monitoring systems are required to provide timely, spatially complete (i.e. mapped), and verifiable information on forest structure (i.e. canopy cover, stand height, and stem volume), biomass, and carbon pools.

Inventory and monitoring of forest conditions (i.e. structure, composition, biomass, and carbon) are often conducted by National Forest Inventory programs that rely upon plot-based field sampling (Tomppo et al., 2010). Measurements from field inventory plots include highly detailed information about forest vegetation composition and structure, from which sample-based estimates of forest conditions can be calculated. Information from inventory plots and other long-term plot networks can be used to develop and calibrate growth and yield equations (Smith, Bell, Herman, & See, 1984; Lessard, McRoberts, & Holdaway, 2001; Lacerte, Larocque, Woods, Parton, & Penner, 2006), and facilitate the calibration and validation of remotely sensed estimates of forest inventory attributes (Smith, 2002; Wulder, Kurz, & Gillis, 2004). The re-measurement of permanent sample plots in a forest inventory cycle can also provide critical information for change monitoring (Poso, 2006; Woodbury, Smith, & Heath, 2007; Herold et al., 2011; Moeur et al., 2011). Despite their widespread use, lack of spatial coverage and lengthy re-measurement intervals can limit the effectiveness of field plots in quantifying forest change, especially in remote and/or unmanaged forests that often have greatly reduced or non-existent field inventory data (Wulder et al., 2004). To accommodate the difficulty and expense in collecting ground plots, photo plots are often used as a substitute for field plots, as well as for stratification purposes in multi-phase plot-based inventory programs (Bechtold & Patterson, 2005; Gillis, Omule, & Brierley, 2005). Photo plots provide an opportunity for implementation of a sample-based inventory upon similar statistical underpinnings as plot-based programs. Large area representation is possible with photo plots (Nielsen, Aldred, & MacLeod, 1979; Magnussen & Russo, 2012); however complete spatial coverage is lacking. Furthermore, establishing and measuring photo plots typically requires purpose collected imagery, which in combination with expert interpretation and the need for some level of supporting field plot data, can substantially increase costs in remote and unmanaged forests.

As a complementary approach to field and photo-based inventories, satellite imagery can provide spatially complete information about forests across large areas. Regional and global maps of forest cover and change over time have long been derived from multispectral satellite imagery (Woodcock et al., 1994; Cohen, Mausersperger, Spies, & Oetter, 2001; Hansen et al., 2003, 2013. Hermosilla, Wulder, White, Coops, & Hobart, 2015a). In particular, Landsat TM/ETM+ imagery is widely used for forest mapping because of its free and open data policy, global coverage, long temporal record, large scene-sizes, and spectral and spatial resolutions compatible with characterizing vegetation conditions and dynamics (Cohen & Goward, 2004; Woodcock et al., 2008; Wulder, Masek, Cohen, Loveland, & Woodcock, 2012a; Kennedy et al., 2014). Regional and national forest inventory programs increasingly integrate satellite imagery with inventory plots, leveraging the detailed forest conditions provided by sampled field or photo plots with complete spatial coverage provided by satellite imagery to generate spatial predictions (e.g. maps) of forest conditions (Ohmann & Gregory, 2002; Tomppo et al., 2008; Wilson, Woodall, & Griffith, 2013; Beaudoin et al., 2014). As one possible approach, nearest neighbor (NN) imputation methods are widely used in plot/imagery integration. Imputation methods fill in observations that are missing for some records (Y-variables), using related variables that are available for all records (X-variables). In forest mapping applications, Y-variables are usually measures of forest composition or structure derived from a sample of field or photo plots, while mapped X-variables can include

multispectral satellite imagery and other spatially complete datasets (i.e. climate, topography). Regression approaches predict new Y-variables when they are missing, but can distort marginal distributions and covariation between Y-variables. In contrast, imputation is a method for filling in missing data by substituting values from donor observations with the underlying assumption that two locations with similar values of X-variables should be similar with respect to Y-variables. A major strength of imputation approaches is these donor-based methods are multivariate, non-parametric, and distribution-free (Eskelson et al., 2009).

Common across large scale imputation mapping projects is the use of satellite imagery as explanatory variables (X-variables). The recent availability of cost-free Landsat images in a consistent, analysis-ready, and easy-to-use format has facilitated a conceptual shift in how Landsat imagery is used in ecosystem inventory, mapping, monitoring (Wulder et al., 2012a; Kennedy et al., 2014). Advances in pixel-based image compositing and change detection using the Landsat time series (LTS) can be especially important for improving the accuracy of forest maps and partially overcoming passive optical imagery limitations. Pixel-based image compositing methods are applied to the Landsat archive to generate cloud-free, radiometrically and phenologically consistent image composites that are spatially contiguous over large areas (Roy et al., 2010; Hansen & Loveland, 2012; Griffiths, van der Linden, Kuemmerle, & Hostert, 2013; White et al., 2014). LTS change detection methods provide pixel-level characterization of forest disturbance, recovery, and other trends (Masek et al., 2008; Huang et al., 2010; Kennedy, Yang, & Cohen, 2010; Hermosilla et al., 2015a). Pixel-based image composites are invaluable for image/plot integration when minimization of year-to-year spectral variability and seamless multi-scene image mosaics are needed to relate to plot data collected across large spatial extents or multiple years (Ohmann et al., 2012). By quantifying disturbance, recovery, and trends, LTS change metrics can improve and partially overcome Landsat limitations in predicting forest vegetation structure (Lu, 2006), because they characterize temporal changes associated with forest processes of mortality, succession, and growth (Pflugmacher, Cohen, & Kennedy, 2012; Zald et al., 2014), and facilitate predictions of forest biomass dynamics over time (Powell et al., 2010; Main-Knorn et al., 2013; Pflugmacher, Cohen, Kennedy, & Yang, 2014).

A more practical approach for large scale inventory in remote areas may be to improve maps of forest attributes using remotely sensed information on vegetation structure. Airborne light detection and ranging (lidar) can provide detailed three-dimensional structure of forest canopies, and has been widely used to characterize forest cover and structure (see reviews by Dubayah & Drake, 2000; Lefsky, Cohen, Parker, & Harding, 2002; Reutebuch, Andersen, & McGaughy, 2005), been integrated with plot-based samples of forest conditions to accurately map forest structure (Hudak, Crookston, Evans, Hall, & Falkowski, 2008; Falkowski et al., 2010; Zald et al., 2014), and used to update forest inventory data (Hilker, Wulder, & Coops, 2008). Declining costs have made lidar acquisitions possible for increasingly large areas; yet complete, single-year wall-to-wall lidar coverage for large areas is still costly and logistically prohibitive for many regional and national forest inventory programs. As a result, the use of lidar in mapping forest conditions is often constrained to sub regional extents (Hudak et al., 2008; Falkowski et al., 2010; Zald et al., 2014), or as a component of multi-phase sampling procedures in larger landscapes (Andersen, Strunk, Temesgen, Atwood, & Winterberger, 2012; Strunk, Temesgen, Andersen, & Packalen, 2014). Alternatively, sample based “lidar plots” may provide detailed, spatially discrete information about vegetation structure, similar to field plots in areas without sufficient field inventory data (Wulder et al., 2012b).

In this paper, we build upon the potential synergies of the Landsat times series and lidar observations to predictively map forest structure (i.e. canopy cover, stand height, basal area, etc.) and aboveground

biomass, bringing together national lidar transect information and wall-to-wall surface reflectance composites developed from LTS imagery within the context of Canada's forest inventory and monitoring needs. Canada's National Forest Inventory (NFI) is a sample-based inventory designed to support many inventory and monitoring needs (Gillis et al., 2005). Extending inventory information to provide spatially explicit and complete information would allow for more accurate assessments, yet financial and logistical constraints limit the number of field and photo plots, particularly in northern forests (Wulder et al., 2004; Falkowski, Wulder, White, & Gillis, 2009). For example, establishing and measuring field inventory plots may be prohibitively expensive and logistically difficult in remote, unmanaged, forests that often lack road access. For unmanaged forest areas, photo plots will typically require purpose collected imagery that are outside of regular forest inventory responsibilities. The collection of aerial photography over remote regions, coupled with needs for expert delineation and interpretation can lead to substantial costs. Our primary objective was to demonstrate the integration of lidar plot data and image composites to predictively map forest structure and aboveground biomass in Canada's forests, using the Province of Saskatchewan as an example. We used detailed lidar plots—sampled observations of forest structure collected from lidar transects—as a surrogate for traditional field and photo plots (Wulder et al., 2012b). We then relate forest conditions from lidar plots to spectral conditions and multi-temporal change

metrics from pixel-based image composites recently developed from Landsat TM/ETM+ imagery for Saskatchewan (White et al., 2014; Hermosilla et al., 2015a), and use nearest neighbor imputation to generate wall-to-wall maps of forest structure and aboveground biomass.

## 2. Methods

### 2.1. Study area

The study area spans 37,881,800 ha of forest and represents 58% of the total area of Saskatchewan (Fig. 1). The study area can be divided into the Taiga Shield, Boreal Shield, Boreal Plains, and Prairies ecozones (Ecological Stratification Working Group, 1996); with the latter being largely unforested. Vegetation in the northern areas is composed primarily of black spruce (*Picea mariana*) and jack pine (*Pinus banksiana*), while forests to the south are characterized by quaking aspen (*Populus tremuloides*), white spruce (*Picea glauca*), and eastern larch (*Larix laricina*). Fire is the primary natural disturbance agent (Kurz & Apps, 1999; Bond-Lamberty, Peckham, Ahl, & Gower, 2007), and in Saskatchewan follows a latitudinal gradient with a higher percentage of annual area burned in the largely unmanaged northern forests (Stocks et al., 2002). In the southern portions of the study area, fires are smaller and less frequent in part due to suppression efforts, while timber harvesting is ongoing in these managed areas (Wulder et al., 2004).

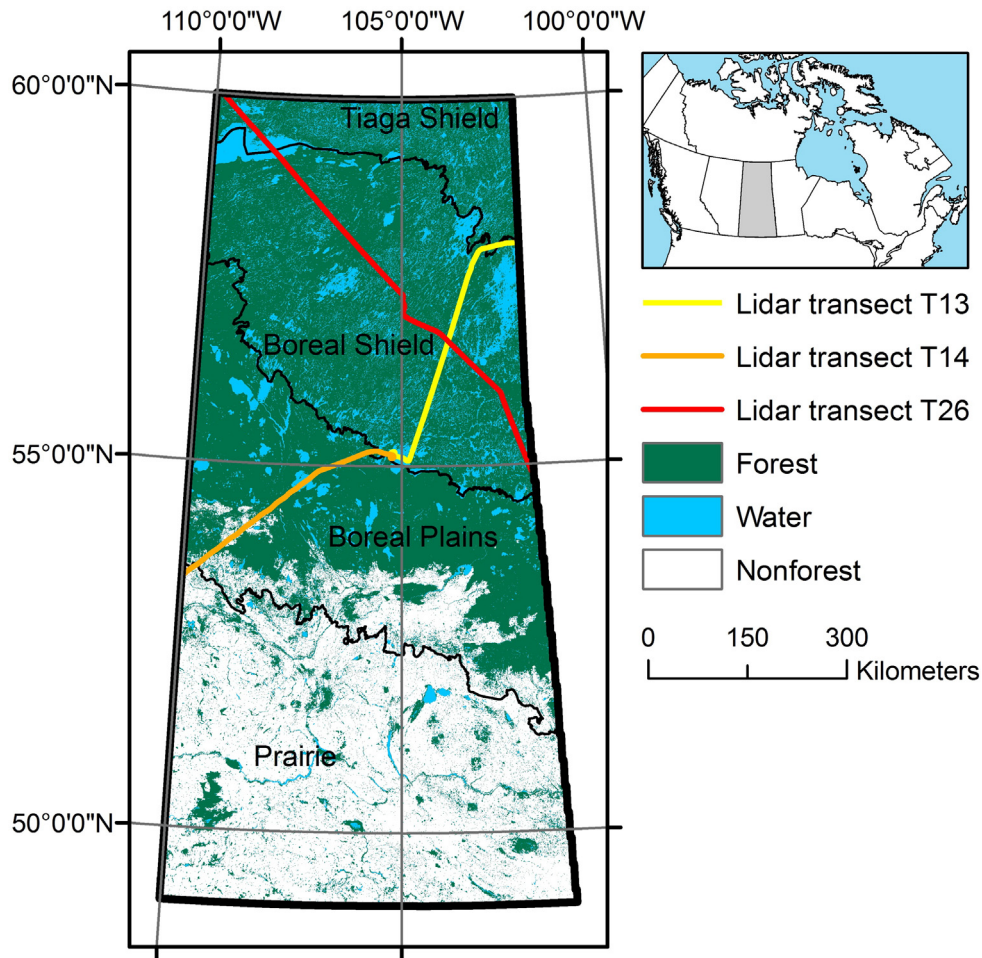


**Fig. 1.** Study area of Saskatchewan depicting dominant land cover types, ecozones, and lidar transects flown in 2010. Areas depicted as forest (green) also include wetlands and shrublands. Forest cover comes from a generalization of Landsat-derived land cover data from the Earth Observation for Sustainable Development of Forests map described in Wulder et al. (2008) and available at <http://tree.pfc.forestry.ca/>. Lidar transect names are associated with national lidar data acquisition (Wulder et al., 2012b). (For interpretation of the references to color in this figure legend, the reader is referred to the web version of this article.)

## 2.2. Lidar data and lidar plot sampling

Lidar data for Saskatchewan was collected in the summer of 2010 along three survey transects with a total length of approximately 1560 km (Fig. 1). These transects are part of a larger national lidar data acquisition of 34 survey transects of more than 25,000 km (Wulder et al., 2012b). Due to the remoteness of Canada's northern forests, survey flights were made between airports with suitable runways, fuel availability, and maintenance facilities. Discrete return lidar data was collected by fixed wing aircraft equipped with an Optech ALTM 3100 laser scanner. Desired survey specifications included a flying height of 1200 m above ground level, 70 kHz pulse rate, scan angle of  $\pm 15^\circ$  from nadir, and a nominal pulse density of 2.8 returns per  $m^2$ . A variety of conditions (adverse weather, extreme terrain, smoke from wildfires, and restricted airspace) required deviations from desired survey specifications (see Wulder et al., 2012b for details).

Lidar survey plots were created by overlaying a  $25 \times 25$  m grid over the lidar transect swaths (~800 m wide), generating over 1.2 million plots, of which 879,482 were forested based on the Landsat-derived land cover data from the Earth Observation for Sustainable Development of Forests map (Wulder et al., 2008, available online at <http://tree.pfc.forestry.ca/>). The 25 m grid for lidar plots was chosen to conform to best practices in application of lidar in support of forest inventory (White et al., 2013). Gridded vegetation metrics (Table 1) characterizing vegetation height, cover, and vertical distribution were calculated for each grid cell from classified lidar point cloud files using the publicly available software FUSION (McGaughey, 2013). In addition to these gridded metrics, additional forest structure variables and total aboveground biomass were predicted for each 25 m cell (Table 1). These predictions were calculated by applying existing and published regression models developed between lidar metrics, forest structure, and aboveground biomass on 201 plots located across Quebec, Ontario, and the Northwest Territories (Wulder et al., 2012b). Application of these regression models resulted in variable predictions, but no error terms or uncertainty in the regression models associated with each prediction.

The 25 m lidar survey plots were sub-sampled to develop training and validation plots for model development, imputation mapping, and accuracy assessment. Sampling occurred as a multi-step process to minimize fine-scale spatial autocorrelation, and avoid potential error and bias associated with higher scan angles at transect edges, small plot sizes, forest edge effects, and mixed structural conditions. A 250 m hexagon lattice was overlain on the lidar transects, and the central 25 m cell within each hexagon was selected as a plot center (Electronic Supplemental Fig. S1). Plot centers were then excluded if they were within 100 m of a lidar transect edge. Lidar plots were then summarized using a  $3 \times 3$  window of 25 m cells (0.5625 ha.), because simulations and empirical research indicate relationships between lidar, field plots, and Landsat imagery decline when plots are smaller than 25 m radius (Frazer, Magnussen, Wulder, & Niemann, 2011; Zald et al., 2014).

Lidar plots were excluded if they contained both disturbed and undisturbed conditions or were within 75 m of a disturbance edge, as determined from the 1984–2012 disturbance history for Saskatchewan (Hermosilla, Wulder, White, Coops, & Hobart, 2015b). Lastly, heterogeneous plots with multiple forest conditions were excluded if the coefficient of variation of vegetation height within plots was greater than 50%. These plots were removed because for heterogeneous plots, explanatory variables are an average of values representing often very different forest attributes, resulting in nearest neighbor predictions closer to the central tendency of the overall sample, over predicting for low values and under predicting for high values. These steps resulted in 4340 lidar plots, of which 75% were randomly sampled for use in model training, and the remaining 25% reserved for model validation. The mean, range, and standard deviation of all lidar metrics and derived structural attributes are presented in Electronic Supplemental Table S1. Summary statistics and frequency distributions were compared between all 879,482 25 m forested cells within the lidar transects and the 4340 lidar plots to ensure sampled lidar plots encompassed the full range of forest structural variability present in the original lidar transects (Electronic Supplemental Table S1, Electronic Supplemental Figs. S2–S3).

## 2.3. Mapped predictor variables and plot-level variable extraction

The primary predictor variables were spectral indices and change metrics derived from Landsat TM/ETM+ imagery, as well as topographic variables (Table 2). Cloud-free, radiometrically and phenologically consistent, and spatially contiguous annual best available pixel (BAP) image composites (White et al., 2014; Hermosilla et al., 2015a) provided surface reflectance data across the province. The forestland in Saskatchewan was represented by 50 scenes (path/rows) of the Landsat Worldwide Referencing System-2 (WRS-2). Candidate images from 1984 to 2012 were identified and downloaded from the USGS Landsat archive as Level-1 Terrain Corrected (L1T) products if they were acquired  $\pm 30$  days of August 1 (Julian day 213) and had less than 70% cloud cover. L1T images were pre-processed to remove clouds, cloud shadows, clear land, and water using Fmask version 2.1 (Zhu & Woodcock, 2012). Surface reflectance and opacity values were generated using LEDAPS 1.3.0 (Schmidt, Jenkerson, Masek, Vermote, & Gao, 2013). Each pixel in every candidate image was given a score based on the 1) sensor type, 2) day of year, 3) distance to cloud or cloud shadow, and 4) opacity. The scoring system originally used by White et al. (2014) was modified by downgrading the sensor score for Landsat 7 ETM+ SLC-off images (from 0.5 to  $-0.7$ ), because geometric fidelity of the Landsat 7 instrument resulted in persistent gaps in the BAP composite if SLC-off data was used in the same area for consecutive years (Hermosilla et al., 2015a). Pixel scores were summed for all L1T candidate images to determine the image with the maximum score at each pixel, BAPs were identified

**Table 1**  
Response variables directly measured or derived from lidar.

Source	Variable	Description	Units
Directly measured from lidar	elev_mean	Mean vegetation height	m
	elev_sd	Standard deviation of vegetation height	m
	elev_cv	Coefficient of variation of vegetation height	%
	elev_p95	95th percentile of vegetation height	m
	cover_2m	Percentage of first returns above 2 m	%
Derived from lidar	cover_mean	Percentage of first returns above mean vegetation height	%
	lorey_height	Lorey's tree height	m
	basal_area	Basal area	$m^2 ha^{-1}$
	stem_volume	Gross stem volume	$m^3 ha^{-1}$
	total_biomass	Total aboveground biomass	$kg^{-1} ha^{-1}$

Note: Derived lidar attributes calculated from equations described by Wulder et al. (2012b) that describe relationships between NFI field plot data and lidar metrics. Basal area and gross stem volume were calculated for trees at 1.3 m above ground level. Total aboveground biomass includes estimates of foliage, branches, crown, bark, wood, and stem biomass.

**Table 2**  
Mapped predictor variables from Landsat spectral indices, change metrics, and topography.

Type	Variable	Description
Spectral indices	TCB	Tasseled cap brightness
	TCG	Tasseled cap greenness
	TCW	Tasseled cap wetness
	TCA	Tasseled cap angle, following Powell, Cohen, Yang, Pierce, and Alberti (2008)
	TCD	Tasseled cap distance, following Duane et al. (2010)
Change metrics	Prechange magnitude variation	Difference in normalized burn ration (NBR) values between breakpoints B and A
	Prechange persistence	Number of years between breakpoints B and A
	Prechange evolution	Ratio of prechange magnitude variation to prechange persistence
	Years since greatest change	Year in which great change breakpoint occurs, subtracted from imputation map year (2010)
	Change persistence	Number of years between breakpoints B and C
	Change magnitude variation	Difference in NBR values between breakpoints B and C
	Change rate	Ratio of change magnitude variation to change persistence
Topography	Postchange magnitude variation	Difference in NBR values between breakpoints D and C
	Postchange persistence	Number of years between breakpoints D and C
	Postchange evolution	Ratio of postchange magnitude variation to postchange persistence
	Elevation	Elevation in meters
	Slope	Slope in degrees
	TSRI	Topographic solar radiation index, following Roberts and Cooper (1989)
	TWI	Topographic wetness index, following Beven and Kirkby (1979)

Note: See Electronic Supplemental Fig. S4 for visual depiction of breakpoints used to generate change metrics.

and assigned, and annual BAP composites generated for 1984 to 2012.

High specificity in user-defined rules can result in data gaps in BAP composites (White et al., 2014). To fill these gaps in a manner that does not confound detection and quantification of changes over time, we used proxy BAP image composites (Hermosilla et al., 2015a) developed in conjunction with multi-temporal change metrics. Initially, outliers from the temporal trajectories for each pixel through the time series were removed using the filtering method described by Kennedy et al. (2010). Then, changes were detected using the Normalized Burn Ratio (NBR, Key & Benson, 2006) as the spectral index, and a variation of the bottom-up breakpoint detection algorithm (Keogh, Chu, Hart, & Pazzani, 2001; Hermosilla et al., 2015a), which divided the time series into temporal trends. Following the generation of breakpoints, a contextual analysis was conducted to improve the consistency and spatial homogeneity of change events, while change events smaller than 0.5 ha were removed. Breakpoints and trends were used to derive metrics that characterize the year, temporal persistence, and spectral magnitude of disturbances (as the difference in NBR values between breakpoints), as well as pre- and post-change conditions (Table 2, Electronic Supplemental Fig. S4). Finally, data gaps were filled with proxy spectral values computed using a piecewise linear interpolation guided by the temporal trends, resulting in seamless proxy BAP composites. From the proxy BAP composites for 2010, we calculated Tasseled Cap indices of brightness (TCB), greenness (TCG), and wetness (TCW) (Crist & Cicone, 1984; Kauth & Thomas, 1976). We also calculated Tasseled Cap angle (TCA) as described by Powell et al. (2008) where  $TCA = \arctan(TCG/TCB)$ , and Tasseled Cap distance (TCD) as described by Duane et al. (2010), where  $TCD = \sqrt{TCG^2 + TCB^2}$ . TCA describes the gradient of percent vegetation cover, whereas TCD is associated with vegetation composition and structure.

Topographic variables used as predictors included elevation, slope, topographic wetness index (TWI), and topographic solar radiation index (TSRI). The digital elevation model comes from the Canadian Digital Elevation Data (CDED, Natural Resources Canada, 1995). The CDED is based on the National Topographic Database (NTDB) digital files with scales ranging from 1:50,000 to 1:250,000. CDED grid spacing is based on geographic coordinates at a maximum and minimum resolution of 0.75 and 3 arc sec for the 1:50,000 scale, and 3 and 12 arc sec for the 1:250,000 scale respectively, depending on latitude. Slope (percent), TWI, and TSRI were calculated from the CDED. The TWI is a model of potential surface moisture, determined by topographic position as described by Beven and Kirkby (1979),

where  $TWI = \ln(\text{specific catchment area}/\tan(\text{slope in radians}))$ . TSRI is a transformed measure of aspect, calculated as described by Roberts and Cooper (1989), where  $TSRI = 1 - \cos((\pi/180)(\text{aspect} - 30))/2$ . TSRI values range from 0 to 1, with a value of 0 indicating cool NE slopes, and 1 indicating warm SW slopes. Elevation, slope, TWI, and TSRI were reprojected and resampled to match the projection and finer 30 m resolution of Landsat pixel composites and change metrics. Mean values for all predictor variables (spectral indices, change metrics, and topographic variables) were extracted for each lidar plot using weighted mean values to account for the different sizes of LiDAR plots and Landsat pixels (Electronic Supplemental Fig. S1).

#### 2.4. Random forest model and imputation mapping

Sampled response variables of forest structure were related to mapped predictor variables of spectral conditions, disturbance history, and topography using the random forest machine learning algorithm (RF), and predictions then were mapped across the study area using nearest neighbor (NN) imputation. RF builds on the functionality of single classification trees (or regression trees for continuous predictions) by extracting a single prediction from an ensemble of tree models (in this case we used 500 trees as a compromise between adequate number of trees while minimizing excessive computational time required for the large number of pixels to be mapped). Each individual classification tree within a RF model is built from a random subset of observations and explanatory variables (Breiman, 2001). There are many statistical methods for relating response and predictor variables in the context of multi-variate imputation mapping, including canonical correlation analysis (Moeur & Stage, 1995), canonical correspondence analysis (Ohmann & Gregory, 2002), and ensemble machine learning methods such as RF (Hudak et al., 2008; Henderson, Ohmann, Gregory, Roberts, & Zald, 2014). One advantage of using RF is its efficiency for high-dimensional data (Prasad, Iverson, & Liaw, 2006), which may be especially important for the hierarchical structure of predictor variables resulting from forest change occurring at different times, magnitudes, directions, and recovery rates.

We built RF models using the R-package 'yalmpute' (Crookston & Finley, 2008). The method implemented in this R-package amalgamates multiple random forest models, each tuned to a single response variable directly measured from lidar (mean, standard deviation, 95th percentile, and coefficient of variation of vegetation height, percent of first returns above 2 m, and percent of first returns above mean). Derived

lidar metrics of forest structure and biomass were attached as ancillary variables to the pixel-level imputation predictions after mapping, meaning these variables are not modeled in RF, but rather joined to the map after plot ids are predicted for each pixel (sensu Zald et al., 2014). We evaluated the relative importance of each predictor variable in the RF model by calculating variable importance scores. For each RF tree the prediction error on the out-of-bag portion of the data is recorded. Then the same is done after permuting each predictor variable. The difference between the two are then averaged over all trees, and normalized by the standard deviation of the differences to generate variable importance scores. To generate spatial predictions (maps), RF chooses neighbor plots based on a non-Euclidean distance measure built from the nodes matrix of the amalgamated RF models. This nodes matrix holds a plot identifier for each terminus (or ‘leaf’) of each classification tree in the RF models. For new locations (map pixels), the terminal nodes where the pixel falls in the RF models are recorded. The nearest-neighbor (kNN = 1) plot for the new pixel is the most frequent plot within its set of nodes. Pixel predictions were made using the RF model and the predict function in the R-package ‘raster’ (Hijmans, 2014).

2.5. Map validation

From the imputation map, predictions of vegetation metrics and forest structure attributes were extracted for map pixels associated with the validation plots using the same methods used to extract values of mapped explanatory variables for training plots. Predictions were compared to observed values using a variety of accuracy measures. We calculated R<sup>2</sup>, root mean squared error (RMSE), and the normalized root mean squared error (nRMSE, RMSE divided by the range of observed values) for each response variable. We also quantified prediction bias and random error using the systematic and unsystematic agreement coefficients (AC<sub>sys</sub> and AC<sub>uns</sub>) following Ji and Gallo (2006). AC<sub>sys</sub> represents the difference between observed and predicted values that can be predicted by a simple linear model (bias from the 1:1 line), and AC<sub>uns</sub> represents differences which appear to be random. In calculating AC<sub>sys</sub> and AC<sub>uns</sub>, geometric mean functional relationships (GMFR) regression lines were used to describe the relationship between the observed and predicted datasets. Unlike ordinary least squares (OLS) regression, GMFR is a symmetric regression model that assumes both X and Y are subject to error.

We assessed the ability of the model to predict ecologically important gradients in forest structure (canopy cover and total aboveground biomass) associated with the magnitude of recent wildfires, as well as the magnitude and years since past wildfires. First, we used the Canadian National Fire Database (CNFDB, Canadian Forest Service, 2013a) to select five large fires (each >30,000 ha, 177,238 ha total) that burned across Saskatchewan in 2008 (no large fires burned in 2009), and had little evidence (<10% of area) of prior fire activity in the preceding century (Electronic Supplemental Fig. S4). Sample points within these selected fire perimeters were generated using a hexagon lattice with 500 m spacing using the function spsample in the R package ‘sp’ (Bivand, Pebesma, & Gomez-Rubio, 2013). From these sample points, 90 \* 90 m polygons were created corresponding to 3 \* 3 cell windows in the imputation map. Polygons were excluded if they contained non-forest land cover or positive change magnitude variation values, because non-forest land cover is beyond the study scope of inference, and positive change polygons are indicative of spatial errors in the fire perimeter database and/or unburned patches within the fire perimeters. Polygon exclusion resulted in 6403 polygons across the five fires. Boxplots were then generated to visualize trends and variation of predicted canopy cover and total aboveground biomass in relation to change magnitude variation.

We also assessed patterns of predicted canopy cover and total aboveground biomass in relation to change magnitude variation and years since fire (0–26 years, corresponding to fires from 1985–2010).

Using the CNFDB, we selected all fires (>500 ha.) that burned between 1985–2010, resulting in 873 fires totaling over 1.5 million ha (Electronic Supplemental Fig. S6). Using the same methods as described above, we sampled points within selected fire perimeters (although with larger 1000 m hexagon spacing), generated 90 \* 90 m sample polygons, and excluded polygons containing non-forest land cover and positive change magnitude variation values. We then binned sample polygons by year of fire (26 bins) and change magnitude variation (6 bins of values ranging from 0 to –1.5 in 0.25 increments), calculated the average predicted cover and biomass values within each bin, and removed bins with fewer than 50 plots, resulting in 16,415 total plots. We then visualized trends in predicted canopy cover and biomass in relation to the years since fire and change magnitude variation using adjacency plots (Wickham, 2009).

3. Results

3.1. Importance of explanatory variables in random forest model

Overall, Tasseled Cap indices (including TC angle and TC distance) and elevation were the most important predictor variables related to our response variables (Fig. 2). The most important change metrics were change magnitude, post-change magnitude, years since greatest change, and post change evolution rate. The topographic variables slope and TWI were also moderately important in the model. Change persistence, pre-change evolution rate, pre-change magnitude, and TSRI had the lowest importance in the model.

3.2. Summary statistics and prediction accuracy on validation plots

Mean predicted values for all forest attributes closely followed mean observed values on validation plots, while the predicted range and standard deviation were slightly but consistently less than observed (Table 3). R<sup>2</sup> values ranged from 0.42 to 0.69, with the highest values for canopy cover (percentage of first returns above 2 m and mean elevation), and the lowest values for vertical variability of vegetation height (elev\_stddev and elev\_cv). Values for nRMSE were consistently low, ranging from 0.08 to 0.14. AC<sub>sys</sub> values were consistently high (indicating low bias), ranging from 0.86 to 0.97, while AC<sub>uns</sub> values were more variable, ranging from 0.18 to 0.63, with less random error for predictions of canopy cover, and greater random error for predictions of vertical variability of vegetation height. For all forest attributes, the model over and under predicts for low and high observed values, respectively (Fig. 3). This bias is most noticeable for derived variables (basal area, gross stem volume, total aboveground biomass), and least noticeable for canopy cover.

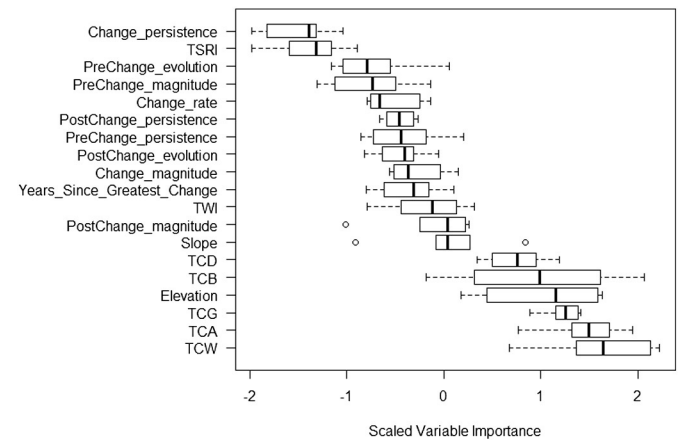


Fig. 2. Scaled importance values of predictor variables from the random forest model of the six lidar metrics of vegetation structure from 3255 training plots in relation to mapped explanatory variables.

**Table 3**  
Summary and accuracy statistics for predicted forest structure variables on 1085 validation plots.

Variable	Units	Observed			Predicted			Accuracy metrics				
		Mean	Range	Stddev	Mean	Range	Stddev	R <sup>2</sup>	RMSE	nRMSE	AC <sub>uns</sub>	AC <sub>sys</sub>
elev_mean	m	5.65	2.28–18.82	2.65	5.54	2.55–17.33	1.97	0.52	1.84	0.11	0.36	0.90
elev_stddev	m	1.85	0.29–8.19	1.10	1.78	0.42–6.11	0.79	0.48	0.80	0.10	0.30	0.86
elev_p95	%	8.72	2.78–26.39	4.01	8.52	3.29–19.09	3.00	0.54	2.74	0.12	0.40	0.90
elev_cv	m	0.32	0.11–0.85	0.08	0.31	0.13–0.87	0.06	0.42	0.06	0.08	0.18	0.90
cover_2m	%	36.35	1.46–97.08	24.10	35.77	2.53–94.4	20.68	0.69	13.45	0.14	0.63	0.97
cover_mean	%	17.86	0.64–55.28	13.02	17.56	0.87–53.18	11.03	0.68	7.34	0.13	0.62	0.97
loreys_height	m	9.77	4.37–22.18	3.15	9.62	4.93–17.52	2.40	0.55	2.11	0.12	0.43	0.91
basal_area	m <sup>2</sup> /ha	11.04	1.6–48.50	7.92	10.66	2.49–36.20	6.00	0.57	5.20	0.11	0.45	0.91
stem_volume	m <sup>3</sup> /ha	39.69	3.26–231.42	36.53	37.81	5.63–158.36	26.67	0.53	24.99	0.11	0.39	0.88
total_biomass	kg/ha	71048.81	4869.12–521957.37	76988.35	67172.29	8358.31–343407.77	54871.18	0.50	54607.22	0.11	0.31	0.86

Note: stdev = standard deviation, RMSE = root mean squared error, nRMSE = normalized root mean squared error, AC<sub>uns</sub> = unsystematic agreement coefficient and AC<sub>sys</sub> = systematic agreement coefficient.

Qualitative analysis of imputation maps also provides a useful assessment of map attributes at multiple spatial scales. Imputation maps of forest structure and total aboveground biomass display clear latitudinal trends at the provincial scale, with higher productivity and forest cover in the southern boreal forest, while the legacy of past wildfires

is clearly identifiable as large areas with reduced cover, height, and biomass (Fig. 4, Electronic Supplemental Figs. S7–S8). At much finer scales, the same imputation maps are spatially consistent with wild-fire perimeters and intra-fire variability, while undisturbed areas

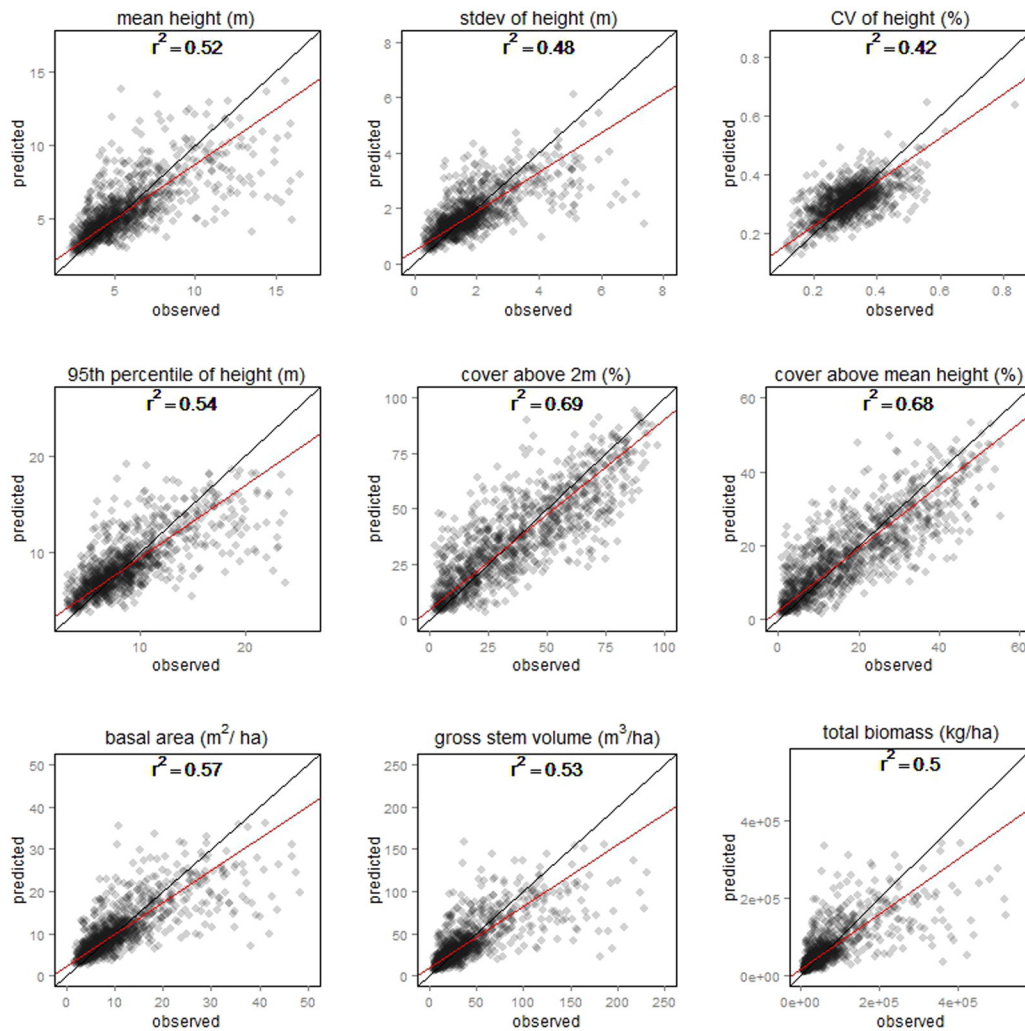


**Fig. 3.** Observed versus predicted values for selected lidar metrics of vegetation structure and derived forest attributes on validation plots (n = 1085). 1:1 line in black, geometric mean functional relationships (GMFRs) between observed and predicted values in red. (For interpretation of the references to color in this figure legend, the reader is referred to the web version of this article.)

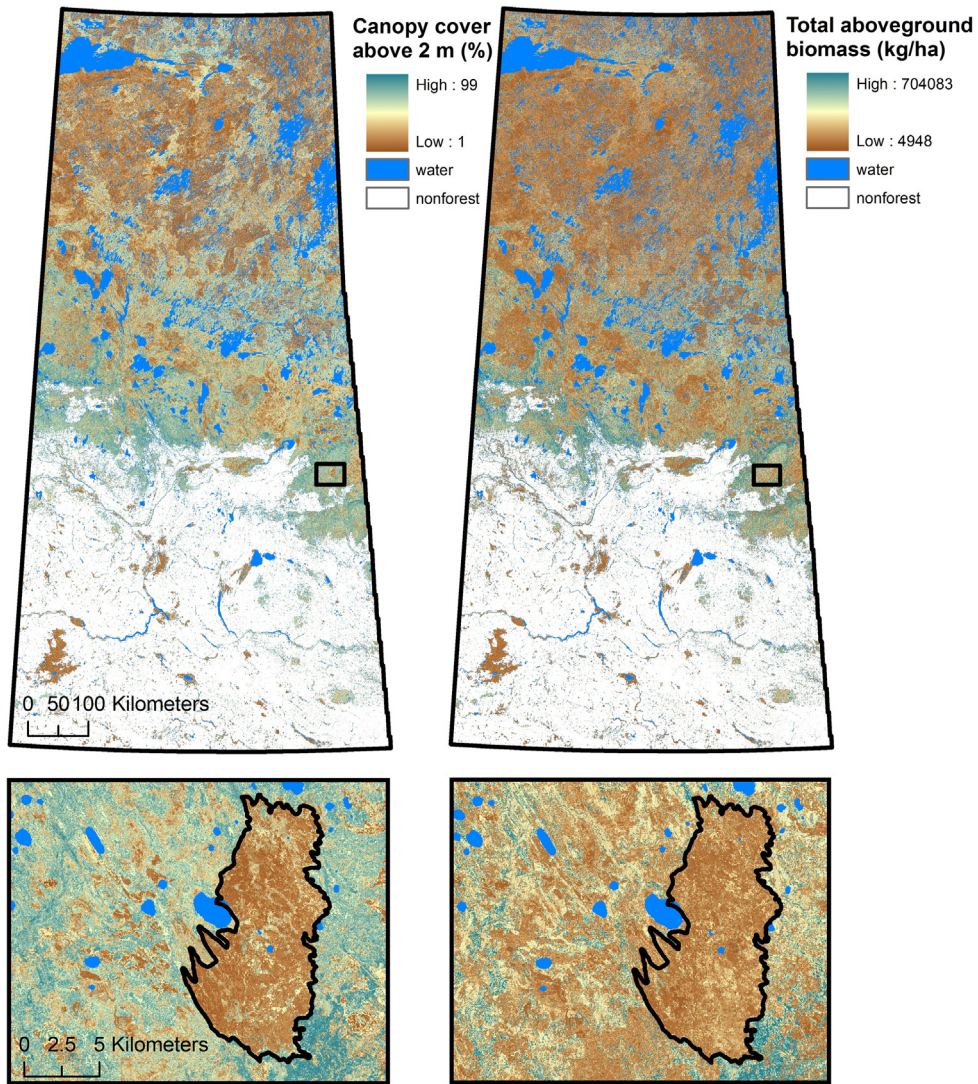


**Fig. 4.** Selected maps of predicted canopy cover above 2 m (percentage of first returns above 2 m), and total aboveground biomass for Saskatchewan. Rectangle in the southern boreal forest associated with bottom images, focused on Leaf fire of 2003 (black outline) and adjacent undisturbed forest. (For interpretation of the references to color in this figure legend, the reader is referred to the web version of this article). See Electronic Supplemental Figs. S7–S8 for provincial maps of other predicted structure variables.

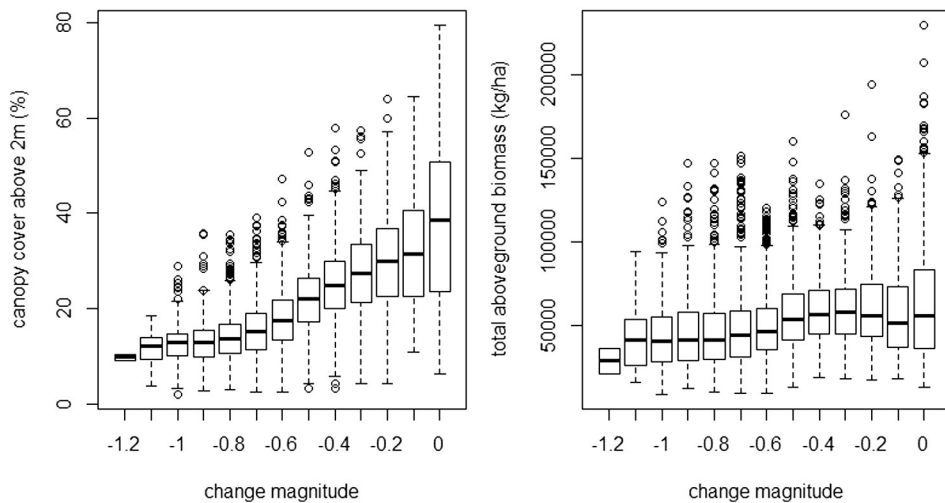


**Fig. 5.** Boxplots of predicted canopy cover above 2 m and total aboveground biomass in relation to change magnitude variation in five wildfires that burned in 2008. See methods section for descriptions of response variables and sampling methods. See Electronic Supplemental Fig. S5 for locations and maps of change magnitude variation for the selected wildfires.



display fine grained patterns likely caused by topographic and edaphic factors.

### 3.3. Predicted canopy cover and total aboveground biomass in relation to past wildfires

Predicted forest canopy cover and total aboveground biomass displayed consistent trends in relation to magnitude change in selected wildfires that burned in 2008 (Fig. 5). High fire severity resulted in consistently low predictions of canopy cover. As change magnitude values approach zero (fire severity declined), both the mean and variability of predicted canopy cover increased. Total aboveground biomass also displayed increased values with lower severity in selected 2008 wildfires, although changes in both mean values and variability of biomass were smaller than those displayed by canopy cover.

Predicted canopy cover and total aboveground biomass also displayed trends in relation to years since wildfire, although these trends covaried with change magnitude, while also being less consistent than found on the selected wildfires that burned in 2008 (Fig. 6). Predicted canopy cover was generally higher with increased years since fire, but the relationship was nonlinear, with variable predictions 16–25 years since fire. Predicted canopy cover increased as change magnitude values approached zero (decreasing fire severity) for more recent fires, but this relationship was not apparent 16–25 years since fire. Predictions of total aboveground biomass were higher with lower fire severity, and this pattern was mostly consistent for 0–25 year old fires. However, biomass predictions showed little trend 0–9 years since fire, after which predicted biomass declined in forests that had experienced high fire severity, and did not appear to decline over time in lower severity fires.

## 4. Discussion

Imputation approaches are widely used for estimating and mapping forest attributes, but the use of lidar as a surrogate for traditional

inventory plots is a new conceptual approach to mapping forest conditions that has seen little application (although see Ahmed, Franklin, Wulder, & White, 2015). While satellite imagery is widely integrated with inventory plots to map forest conditions, pixel composites and change metrics have only recently become available for large areas, so their use as explanatory variables in mapping forest conditions is less common (Pflugmacher et al., 2014; Zald et al., 2014). A key finding of this study is that lidar plots can be used as a surrogate for traditional field inventory plots for imputation mapping applications. Below we discuss the ability of our mapping approach to predict forest structure and biomass and spatially characterize key ecological patterns and processes. We also discuss the value of pixel composites and change metrics derived from Landsat TM/ETM+ imagery in the context of imputation mapping. While lidar plots have great potential in forest mapping applications, there are important limitations and uncertainty we discuss that may be inherent to lidar plots, the transect sampling utilized in this study, and imputation procedures.

### 4.1. Statistical and ecological validity of imputation maps

When combined with spectral and change information from Landsat time series imagery, plot-level predictions of many forest attributes have comparable or superior accuracy to other regional-scale imputation mapping projects that use traditional field plots and satellite imagery. For example, our estimates of basal area were equal or more accurate ( $R^2 = 0.57$ ) than imputation maps generated in Oregon and California using traditional inventory plots and Landsat imagery without change metrics ( $R^2 = 0.16–59$ ) (Ohmann & Gregory, 2002; Pierce, Ohmann, Wimberly, Gregory, & Fried, 2009; Zald et al., 2014). Likewise, our estimates of total aboveground biomass have plot-level accuracy comparable to recent imputation mapping of Canada's forest using photo plots and moderate resolution MODIS imagery (Beaudoin et al., 2014). These comparisons to other studies are partially confounded by different statistical methods, inventory protocols, and forest types; yet they indicate lidar plots can be used at least as accurately as traditional

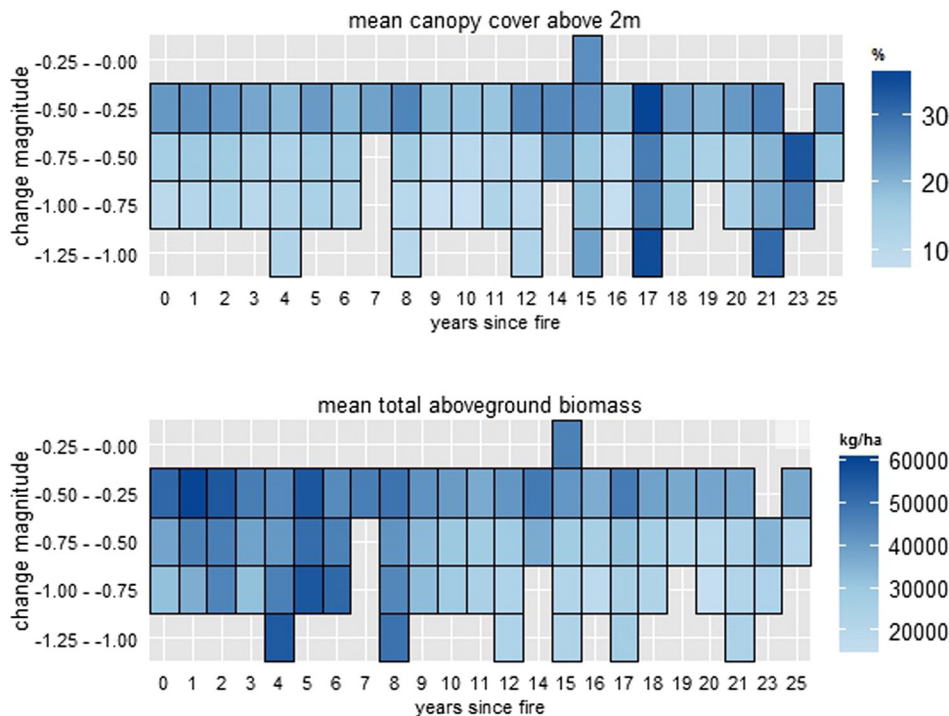


**Fig. 6.** Predicted canopy cover (percentage of first returns above 2 m) and total aboveground biomass in relation to change magnitude and years since wildfire. Combinations of a given change magnitude class and years since fire with fewer than 50 plots have been excluded. More negative change magnitude values indicate higher burn severity. (For interpretation of the references to color in this figure legend, the reader is referred to the web version of this article). See the methods section for descriptions of response variables and sampling of wildfires. See Electronic Supplemental Fig. S6 for a map of wildfires sampled.

field and photo inventory plots to predict and map forest structure and total aboveground biomass.

In addition to plot-level accuracy assessments, our spatial predictions of forest attributes appear to be ecologically realistic, quantifying dominant ecological patterns and processes. In the ecozones containing most of Saskatchewan's forests (Tiaga Shield, Boreal Shield, Boreal Plains), fire is the dominant disturbance agent shaping ecosystem dynamics (Kurz & Apps, 1999; Bond-Lamberty et al., 2007). We found that in recent fires, predicted canopy cover and total aboveground biomass were negatively associated with increased fire severity, consistent with known relationships of these forest attributes to burn severity (Campbell, Donato, Azuma, & Law, 2007; Miller et al., 2009). Predicted total aboveground biomass was less sensitive than canopy cover to fire severity, which should be expected since trees have lower combustion factors compared to litter and soil, resulting in tree biomass largely remaining in forests via transfer from living to dead biomass pools (i.e. snags and logs), and a larger portion of pyrogenic emissions to the atmosphere coming from combusted litter and soil (Campbell et al., 2007). Trends in predicted canopy cover and total aboveground biomass were more variable across 25 years of fires, but were relatively consistent with post-fire vegetation recovery. For example, the relationship of canopy cover and burn severity is much stronger in the initial years after wildfire, but this relationship weakens over time as forests recover, consistent with post-fire spectral trajectories of forest recovery over time (Goetz, Fiske, & Bunn, 2006). More difficult to explain are predictions of total aboveground biomass that do not decline until approximately eight years after wildfires, and then are variable but have largely stopped declining 15 years after fire. These trends may result from how post-fire tree mortality, snag fall, and vegetation recovery dynamics are reflected in lidar metrics such as canopy cover and mean vegetation height used to derive biomass estimates (Bolton, Coops, & Wulder, 2015). Dead trees (snags) can persist for many years after fire (Russell, Saab, Dudley, & Rotella, 2006; Angers, Drapeau, & Bergeron, 2010; Dunn & Bailey, 2012), resulting in lidar metrics of canopy height remaining elevated until the majority of snags within a pixel fall or experience significant breakage. Later in post-fire recovery, snagfall-driven reductions in stand height may be partially offset by increases in canopy cover and vegetation height associated with tree regeneration and growth. The stability of lidar vegetation metrics may be consistent with temporal lags of tree mortality and snag fall in post-fire forest dynamics, but they may also represent a source of error where the model is unable to distinguish living trees and snags with similar stand heights, even with inclusion of Landsat-derived disturbance history.

#### 4.2. Importance of pixel composites and change metrics in imputation mapping

Pixel composites and change metrics derived from Landsat TM/ETM+ imagery were an important component of the imputation method used in this study. Spatially complete, cloud-free, and radiometrically consistent surface reflectance image composites support the development of spatially complete and consistent predictions of forest attributes, regardless of the statistical methods or plot data used. The opening of the Landsat archive and development of best available pixel (BAP) compositing methods have greatly improved the development of cloud-free image mosaics with the holdings for Canada being spatially and temporally comprehensive (White & Wulder, 2013); notwithstanding the favorable coverage of present data, gaps remain on an annual basis necessitating the development and use of proxy image composites (White et al., 2014; Hermosilla et al., 2015a). With the launch of Landsat 8 in 2013, Landsat OLI imagery is acquired in a denser and more globally consistent manner than Landsat TM/ETM+ (Roy et al., 2014), which should greatly increase the density of cloud-free scenes. Furthermore, the successful launch of the Sentinel 2 mission by the European Space Agency, with similar spatial and spectral characteristics to Landsat (Drusch et al., 2012), will greatly increase the

temporal density of imagery available in the future. Despite current and future improvements with Landsat 8 and Sentinel 2, pixel compositing will continue to be necessary for forest inventory and monitoring applications for both historical and future imagery, not only in Canada, but also for other boreal and tropical regions with persistent cloud cover, snow cover, and short phenologic windows (Asner, 2001; Potapov, Turubanova, & Hansen, 2011).

Previous studies have demonstrated the benefits of incorporating multi-temporal change metrics from Landsat imagery to improve predictions of forest structure and biomass (Pflugmacher et al., 2012, 2014; Zald et al., 2014; Ahmed et al., 2015). However, scaling up from these smaller proof of concept studies has been limited by the availability of change metrics at regional and national scales. We leveraged the recent availability of change metrics and proxy pixel composites for Saskatchewan (Hermosilla et al., 2015a, 2015b). Landsat pixel compositing and multi-temporal change metrics are an area of active research and product development. The specific image products used in this study are not nationally or globally available, yet the emergence of similar national and global image composites and change metrics (Roy et al., 2010; Hansen et al., 2013) suggests multi-temporal change mapping will be increasingly available to support regional and national forest inventory programs. In addition to multi-temporal change detection, imputation mapping of forest conditions may greatly benefit from recent advances in change attribution (Kennedy et al., 2015; Hermosilla et al., 2015b). Change attribution may improve prediction accuracy by distinguishing pixel-level spectral conditions, year of change, and magnitude of change that can be very similar for different disturbance agents (for example harvesting versus wildfire), yet these disturbances can result in very different forest structure and biomass. In northern Saskatchewan, change attribution may be less important because fire is the dominant disturbance agent. However, the increased importance of other disturbance agents such as harvesting may lower prediction accuracy in disturbed forests in southern Saskatchewan, and this issue may be especially important in other forest regions with multi-agent disturbance regimes.

#### 4.3. Limitations of lidar plots in imputation mapping

A key component of this study is the use of lidar plots as surrogates for traditional field plots within the imputation technique. This novel element also poses conceptual and methodological limitations for accuracy assessment, uncertainty analysis, and large area estimation of forest resources. The most obvious limitation is the inability to map species composition, because lidar plots lack tree observations that include species identification, and this limitation also applies to any variable that is only observable with field plot data. Imputation mapping relies on relationships between sampled response and mapped predictor variables, constraining predictions to values in the plot sample, so that predictions cannot exceed biological reality as determined from the sample dataset. However, this assumes the sample dataset adequately contains the variables of interest, and represents the range of variation in these variables that are unmeasured in the larger study area. Plot-level accuracy assessments used a validation set of sampled lidar plots spatially constrained within lidar transects. Sampled lidar plots cover the range and frequency distribution of values in the larger lidar transects (Electronic Supplemental Table S2, Electronic Supplemental Figs. S2–S3), but meaningful plot-level validation of predicted forest attributes beyond the lidar transects was precluded by the scarcity of available inventory field plots in the study area, as Provincial and industry inventory data exist, but were not available at the time of this study. Our mean predictions of aboveground biomass for the Boreal Shield (56.47 tons/ha) and Boreal Plains (104.30 tons/ha) ecozones are reasonable when compared to provincial-level estimates derived from National Forest Inventory plots (e.g., 75.6 tons/ha for Boreal Shield and 77.7 tons/ha for Boreal Plains) (Canadian Forest Service, 2013b), but these comparisons have significant caveats. NFI-based biomass estimates incorporate all plot-

data for entire ecozones, which extend beyond the boundaries of Saskatchewan and our study area. Moreover, NFI plot density is low for these ecozones (290 for the Boreal Shield, 116 for the Boreal Plains), and entirely lacking for the Taiga Shield and Prairies ecozones. For the two ecozones with NFI data, our maximum biomass estimates are 56 and 59% higher than NFI estimates. However, natural and anthropogenic disturbances prevent most forests from reaching their maximum potential biomass, posing problems for establishing upper bounds using geographically systematic inventory plots (Smithwick, Harmon, Remillard, Acker, & Franklin, 2002), and this issue is compounded by low plot sample numbers in Canada's unmanaged northern forests.

Plot-level accuracy assessments did find a consistent bias, over predicting all attributes at low observed values and under predicting at high values. Under prediction for high observed values is also found in studies relating traditional field inventory plots and space borne lidar to Landsat spectral conditions (Ohmann & Gregory, 2002; Duncanson, Niemann, & Wulder, 2010), consistent with saturation of Landsat reflectance data in forests with high biomass and leaf area index. Prediction biases may also be caused to varying degrees by the lidar data, lidar plot sampling procedures, and nearest neighbor methodology. Lidar data within a 25 m pixel was only used if the percent of first returns above 2 m was greater than zero, resulting in exclusion of lidar data that may represent forest conditions found in canopy gaps, forest openings, and recent harvests. Heterogeneous plots with multiple forest conditions were excluded, but this reduced the frequency of lidar plots with very low canopy cover (Electronic Supplemental Fig. S3). Finally, the nearest neighbor imputation method itself may contribute to prediction bias. Lidar plots occupy a multi-dimensional cloud within the feature space of the explanatory variables, with longer nearest neighbor distances towards the edges of the plot cloud. Therefore, pixels towards the edges of the feature space are more likely to have larger nearest neighbor distances and their nearest neighbor plots are more likely to be towards the centroid of the feature space, resulting in over and under predictions at the low and high ranges, respectively. While beyond the scope of this study, these biases may be partially corrected by approaches that stratify plot selection during sampling or imputation procedures (McRoberts & Tomppo, 2007; Eskelson, Temesgen, & Barrett, 2008). However, using the plots themselves to derive strata can potentially violate the assumption that plots are a random sample of a stratum, this can be a particular concern when using nearest neighbor imputation techniques (McRoberts & Tomppo, 2007), requiring other independent data sources for stratification purposes.

In addition to limitations for plot-level accuracy assessment, spatially clustered lidar plots from transects may require new conceptual and methodological approaches to spatial accuracy assessment, area estimation, and uncertainty analysis. Geographically systematic sampling underlies assessment protocols for continuous geospatial datasets such as imputation maps of forest conditions (Riemann, Wilson, Lister, & Parks, 2010), yet the lidar transects we use are not a spatially systematic probability sample. Additionally, derived lidar attributes such as stem volume and biomass are themselves not true observations but predictions derived from regressions between lidar and values from NFI field plots, posing questions for using accuracy assessments protocols that compare observed and predicted values. While posing problems for accuracy assessments, the transect based sample we use is more widely distributed spatially and much larger than is typically used in global studies of Lefsky (2010) and Simard, Pinto, Fisher, and Baccini (2011), as summarized in Bolton, Coops, and Wulder (2013). Furthermore, field plot based studies are often limited in the number of samples available and are often spatially limited to safe and ready access to road networks, which would adversely constrain and bias plot sampling in Northern Canada, as well as many regions with remote and inaccessible forests.

Nearest neighbor distance maps can provide an indirect metric of spatial error in map predictions (Ohmann & Gregory, 2002; Beaudoin et al., 2014), but they do not provide direct measures of error associated

with the predicted forest conditions of interest. Limitations of spatial accuracy assessment also pose problems for area estimation and uncertainty analysis. For example, from our predictions we can generate total estimates of basal area (365.68 M m<sup>2</sup>), timber volume (1321.90 M m<sup>3</sup>), and total aboveground biomass (2.36 Pg) for Saskatchewan, yet we have limited tools for quantifying the uncertainty of such estimates. One approach to quantify uncertainty would be to apply recently developed variance estimators to imputation predictions, but the computational requirements to calculate variance estimates may be prohibitive when using the NN imputation approach over large areas (McRoberts, Tomppo, Finley, & Heikkinen, 2007). There are other approaches that have recently been developed to quantify variance in univariate regressions (Gregoire et al., 2011; Ståhl et al., 2011) and uncertainty in multivariate imputation procedures (Bell, Gregory, & Ohmann, 2015), and development of such procedures for Random Forest implementations of imputation procedures is an area of future research.

More fundamentally, a major area for future research is to assess how completely lidar plots from transects occupy the feature space of the larger study area of interest, as well as covering the variation of the forest variables of interest. Such knowledge could be used with a priori flight information to plan optimal locations for lidar transects, as well as after lidar collection to determine if additional lidar is needed, quantify areas with diminished plot support, and stratify lidar plot sampling and model based estimation. Regardless of these potential limitations, it is important to recognize the lidar plot sample size used in this study is larger and better distributed than could be expected from a field based program over the same jurisdiction.

Derived forest attributes (basal area, stem volume, total aboveground biomass, etcetera) also have important sources of error and limitations for quantifying their uncertainty. These attributes were calculated using empirical models developed between lidar plots and 201 NFI inventory plots across Canada's boreal forest (Wulder et al., 2012b). Model fit for these attributes was high (adjusted R<sup>2</sup> of 0.64–0.84), and our imputation models only use the predicted values from these equations. It is possible to incorporate the uncertainty or confidence intervals from the Wulder et al. (2012b) models into pixel-level imputation predictions as ancillary variables, but there are important reasons why we did not. Most importantly, equations from Wulder et al. (2012b) were developed across multiple ecozones and provinces in order to have a robust NFI plot sample size and nationally consistent equations. While model fit and lidar metrics used as predictor variables are generally consistent with other studies (Hudak et al., 2006; Li, Andersen, & McGaughey, 2008), applying confidence intervals from national models to an area without robust plot support is likely exceeding the data's scope of inference. More broadly, calculating basal area, stem volume, and total aboveground biomass is limited by multiple sources of error. For example, tree species vary in their wood density and canopy structure, and these species-level differences influence biomass equations (Lambert, Ung, & Raulier, 2005; Ung, Bernier, & Guo, 2008; Jenkins, Chojnacky, Heath, & Birdsey, 2003), yet we do not incorporate tree species into our predictions. However, Tompalski, Coops, White, and Wulder (2014) found error in height had a larger impact than species information on simulated tree volume estimates, implying our lidar based models of forest structure are likely more accurate than estimates generated with species data but without precise lidar height estimates. Furthermore, field-based biomass estimates themselves have many sources of sampling and measurement error, as well as model misspecifications (Temesgen, Affleck, Poudel, Gray, & Sessions, 2015). One of the strengths of our imputation approach is we only used lidar metrics (canopy height, variation of canopy height, and canopy cover) as response variables in the Random Forest model, while derived forest attributes with higher potential but unquantified uncertainty and error were predicted as ancillary variables. This approach is inherently more flexible as it allows future incorporation of more accurate predictions as new models of the derived forest attributes become available.

## 5. Conclusions

Canada's National Forest Inventory (NFI) is designed to support many inventory, monitoring, and reporting objectives. As a sample based program, the NFI represents 100% of Canada's forest with a 1% sample (Gillis et al., 2005), resulting in a need to characterize and map forest conditions on the remaining 99%. This information must be temporally and nationally consistent, spatially explicit and exhaustive, at a spatial resolution that can resolve natural and human impacts, and generated in a way that is transparent and scientifically defensible. Approaches that integrate inventory plots with remotely sensed imagery have commonly had limitations in the context of Canada's extensive northern forests (i.e. too few inventory plot samples, temporal mismatch of plots and imagery, and now-mitigated issues with multi-scene Landsat mosaics). By integrating lidar plots with Landsat pixel composites and change metrics, our approach overcomes many of these limitations to provide timely, spatially complete, and verifiable information on forest conditions. This information can inform policy, support jurisdictional (including national) monitoring programs, and facilitate a wide range of scientific inquiry. Furthermore, lidar-based imputation of forest attributes is temporally transferable (Fekety, Falkowski, & Hudak, 2015), indicating that the single year predictions we present in this study can be extended across the Landsat time series to characterize multi-decadal changes in forest conditions.

## Acknowledgments

This research was undertaken as part of the "National Terrestrial Ecosystem Monitoring System (NTEMS): Timely and detailed national cross-sector monitoring for Canada" project was jointly funded by the Canadian Space Agency (CSA) Government Related Initiatives Program (GRIP) and the Canadian Forest Service (CFS) of Natural Resources Canada.

## Appendix A. Supplementary data

Supplementary data to this article can be found online at <http://dx.doi.org/10.1016/j.rse.2016.01.015>.

## References

- Ahmed, O. S., Franklin, S. E., Wulder, M. A., & White, J. C. (2015). Characterizing stand-level forest canopy cover and height using Landsat time series, samples of airborne lidar, and the Random Forest algorithm. *ISPRS Journal of Photogrammetry and Remote Sensing*, *101*, 89–101.
- Andersen, H. -E., Strunk, J., Temesgen, H., Atwood, D., & Winterberger, K. (2012). Using multilevel remote sensing and ground data to estimate forest biomass resources in remote regions: A case study in the boreal forests of interior Alaska. *Canadian Journal of Remote Sensing*, *37*, 596–611.
- Angers, V. A., Drapeau, P., & Bergeron, Y. (2010). Snag degradation pathways of four North American boreal tree species. *Forest Ecology and Management*, *259*, 246–256.
- Asner, G. P. (2001). Cloud cover in Landsat observation of the Brazilian Amazon. *International Journal of Remote Sensing*, *22*, 3855–3862.
- Beaudoin, A., Bernier, P. Y., Guindon, L., Villemaire, P., Guo, X., Stinson, G., ... Hall, R. J. (2014). Mapping attributes of Canada's forests at moderate resolution through kNN and MODIS imagery. *Canadian Journal of Forest Research*, *44*, 521–532.
- Bechtold, W. A., & Patterson, P. L. (2005). The enhanced forest inventory and analysis program: National sampling design and estimation procedures. *USDA Forest Service Southern Research Station General Technical Report SRS-80*. Asheville, NC.
- Bell, D. M., Gregory, M. J., & Ohmann, J. L. (2015). Imputed forest structure uncertainty varies across elevational and longitudinal gradients in the western Cascade Mountains, Oregon USA. *Forest Ecology and Management*, *358*, 154–164.
- Beven, K. J., & Kirkby, M. J. (1979). A physically based, variable contributing area model of basin hydrology. *Hydrological Sciences Bulletin*, *24*, 43–69.
- Bivand, R. S., Pebesma, E., & Gomez-Rubio, V. (2013). *Applied spatial data analysis with R* (2nd ed.). NY: Springer.
- Bolton, D. K., Coops, N. C., & Wulder, M. A. (2013). Investigating the agreement between global canopy height maps and airborne Lidar derived height estimates over Canada. *Canadian Journal of Remote Sensing*, *39*(s1), S139–S151. <http://dx.doi.org/10.5589/m13-036>.
- Bolton, D. K., Coops, N. C., & Wulder, M. A. (2015). Characterizing residual structure and forest recovery following high-severity fire in the western boreal of Canada using Landsat time-series and airborne lidar data. *Remote Sensing of Environment*, *163*, 48–60.
- Bond-Lamberty, B., Peckham, S. D., Ahl, D. E., & Gower, S. T. (2007). Fire as the dominant driver of central Canadian boreal forest carbon balance. *Nature*, *450*, 89–92.
- Breiman, L. (2001). Random forests. *Machine Learning*, *45*, 5–32.
- Campbell, J., Donato, D., Azuma, D., & Law, B. (2007). Pyrogenic carbon emission from a large wildfire in Oregon, United States. *Journal of Geophysical Research: Biogeosciences (2005–2012)*, *112*(G4).
- Canadian Forest Service (2013a). Canadian national fire database – Agency fire data. Natural Resources Canada, Canadian Forest Service, Northern Forestry Centre, Edmonton, Alberta. Accessed online 25 May 2015 at [http://cwfs.cfs.nrcan.gc.ca/en\\_CA/nfdb](http://cwfs.cfs.nrcan.gc.ca/en_CA/nfdb)
- Canadian Forest Service (2013b). Canada's National Forest Inventory, revised 2006 baseline (version 3, December 2013). Accessed online 25 May 2015 at <http://nfi.nfis.org>
- Cohen, W. B., & Goward, S. N. (2004). Landsat's role in ecological applications of remote sensing. *Bioscience*, *54*, 535–545.
- Cohen, W. B., Maersperger, T. K., Spies, T. A., & Oetter, D. R. (2001). Modelling forest cover attributes as continuous variables in a regional context with thematic mapper data. *International Journal of Remote Sensing*, *22*, 2279–2310.
- Crist, E. P., & Cicone, R. C. (1984). Application of the tasseled cap concept to simulated thematic mapper data (transformation for MSS crop and soil imagery). *Photogrammetric Engineering and Remote Sensing*, *50*, 343–352.
- Crookston, N. L., & Finley, A. O. (2008). yalmpute: An R package for kNN imputation. *Journal of Statistical Software*, *23*, 1–16.
- Daily, G. (1997). *Nature's services: societal dependence on natural ecosystems*. Island Press.
- Drusch, M., Del Bello, U., Carlier, S., Colin, O., Fernandez, V., Gascon, F., ... Bargellini, P. (2012). Sentinel-2: ESA's optical high-resolution mission for GMES operational services. *Remote Sensing of Environment*, *120*, 25–36.
- Duane, M. V., Cohen, W. B., Campbell, J. L., Hudiburg, T., Turner, D. P., & Weyeremann, D. L. (2010). Implications of alternative field-sampling designs on Landsat-based mapping of stand age and carbon stocks in Oregon forests. *Forest Science*, *56*, 405–416.
- Dubayah, R. O., & Drake, J. B. (2000). Lidar remote sensing for forestry. *Journal of Forestry*, *98*, 44–46.
- Duncanson, L. I., Niemann, K. O., & Wulder, M. A. (2010). Integration of GLAS and Landsat TM data for aboveground biomass estimation. *Canadian Journal of Remote Sensing*, *36*, 129–141.
- Dunn, C. J., & Bailey, J. D. (2012). Temporal dynamics and decay of coarse wood in early seral habitats of dry-mixed conifer forests in Oregon's Eastern Cascades. *Forest Ecology and Management*, *276*, 71–81.
- Ecological Stratification Working Group (1996). A National ecological framework for Canada. *Ottawa/Hull. Agriculture and Agri-Food Canada, Research Branch, Centre for Land and Biological Resources Research, and Environment Canada, State of the Environment Directorate, Ecozone Analysis Branch*.
- Eskelson, B. N., Temesgen, H., & Barrett, T. M. (2008). Comparison of stratified and non-stratified most similar neighbor imputation for estimating stand tables. *Forestry*, *81*, 125–134.
- Eskelson, B. N., Temesgen, H., Lemay, V., Barrett, T. M., Crookston, N. L., & Hudak, A. T. (2009). The roles of nearest neighbor methods in imputing missing data in forest inventory and monitoring databases. *Scandinavian Journal of Forest Research*, *24*, 235–246.
- Falkowski, M. J., Hudak, A. T., Crookston, N. L., Gessler, P. E., Uebler, E. H., & Smith, A. M. S. (2010). Landscape-scale parameterization of a tree-level forest growth model: A k-nearest neighbor imputation approach incorporating LIDAR data. *Canadian Journal of Forest Research*, *40*, 184–199.
- Falkowski, M. J., Wulder, M. A., White, J. C., & Gillis, M. D. (2009). Supporting large-area, sample-based forest inventories with very high spatial resolution satellite imagery. *Progress in Physical Geography*, *33*, 403–423.
- Fekety, P. A., Falkowski, M. J., & Hudak, A. T. (2015). Temporal transferability of LiDAR-based imputation of forest inventory attributes. *Canadian Journal of Forest Research*, *45*, 422–435.
- Food and Agriculture Organization of the United Nations [FAO] (2010A). *Global forest resources assessment 2010: Main report*. Food and Agriculture Organization of the United Nations.
- Frazer, G., Magnussen, S., Wulder, M., & Niemann, K. (2011). Simulated impact of sample plot size and co-registration error on the accuracy and uncertainty of LiDAR-derived estimates of forest stand biomass. *Remote Sensing of Environment*, *115*, 636–649.
- Gillis, M., Omule, A., & Brierley, T. (2005). Monitoring Canada's forests: The national forest inventory. *The Forestry Chronicle*, *81*, 214–221.
- Goetz, S. J., Fiske, G. J., & Bunn, A. G. (2006). Using satellite time-series data sets to analyze fire disturbance and forest recovery across Canada. *Remote Sensing of Environment*, *101*, 352–365.
- Gregoire, T. G., Ståhl, G., Næsset, E., Gobakken, T., Nelson, R., & Holm, S. (2011). Model-assisted estimation of biomass in a LiDAR sample survey in Hedmark County, Norway. *Canadian Journal of Forest Research*, *41*, 83–95.
- Griffiths, P., van der Linden, S., Kuemmerle, T., & Hostert, P. (2013). Pixel-based Landsat compositing algorithm for large area land cover mapping. *IEEE Journal of Selected Topics in Applied Earth Observations and Remote Sensing*, *6*, 2088–2101.
- Hansen, M. C., & Loveland, T. R. (2012). A review of large area monitoring of land cover change using Landsat data. *Remote Sensing of Environment*, *122*, 66–74.
- Hansen, M. C., Defries, R. S., Townshend, J. R. G., Carroll, M., Dimiceli, C., & Sohlberg, R. A. (2003). Global percent tree cover at a spatial resolution of 500 meters: First results of the MODIS vegetation continuous fields algorithm. *Earth Interactions*, *7*, 1–15.
- Hansen, M. C., Potapov, P. V., Moore, R., Hancher, M., Turubanova, S., Tyukavina, A., ... Loveland, T. (2013). High-resolution global maps of 21st-century forest cover change. *Science*, *342*, 850–853.
- Henderson, E. B., Ohmann, J. L., Gregory, M. J., Roberts, H. M., & Zald, H. (2014). Species distribution modelling for plant communities: Stacked single species or multivariate modelling approaches? *Applied Vegetation Science*, *17*, 516–527.

- Hermosilla, T., Wulder, M. A., White, J. C., Coops, N. C., & Hobart, G. W. (2015a). An integrated Landsat time series protocol for change detection and generation of annual gap-free surface reflectance composites. *Remote Sensing of Environment*, 158, 220–234.
- Hermosilla, T., Wulder, M. A., White, J. C., Coops, N. C., & Hobart, G. W. (2015b). Regional detection, characterization, and attribution of annual forest change from 1984 to 2012 using Landsat-derived time-series metrics. *Remote Sensing of Environment*, 170, 121–132.
- Herold, M., Román-Cuesta, R. M., Mollicone, D., Hirata, Y., Van Laake, P., Asner, G. P., ... MacDicken, K. (2011). Options for monitoring and estimating historical carbon emissions from forest degradation in the context of REDD+. *Carbon Balance and Management*, 6, 1–7.
- Hijmans, R. J. (2014). Raster: Geographic data analysis and modeling. *R package version 2.2–31* (Accessed online 25 May 2015 at <http://CRAN.R-project.org/package=raster>).
- Hilker, T., Wulder, M. A., & Coops, N. C. (2008). Update of forest inventory data with lidar and high spatial resolution satellite imagery. *Canadian Journal of Remote Sensing*, 34, 5–12.
- Huang, C., Goward, S. N., Masek, J. G., Thomas, N., Zhu, Z., & Vogelmann, J. E. (2010). An automated approach for reconstructing recent forest disturbance history using dense Landsat time series stacks. *Remote Sensing of Environment*, 114, 183–198.
- Hudak, A. T., Crookston, N. L., Evans, J. S., Falkowski, M. J., Smith, A. M., Gessler, P. E., & Morgan, P. (2006). Regression modeling and mapping of coniferous forest basal area and tree density from discrete-return lidar and multispectral satellite data. *Canadian Journal of Remote Sensing*, 32, 126–138.
- Hudak, A. T., Crookston, N. L., Evans, J. S., Hall, D. E., & Falkowski, M. J. (2008). Nearest neighbor imputation of species-level, plot-scale forest structure attributes from LiDAR data. *Remote Sensing of Environment*, 112, 2232–2245.
- Jenkins, J., Chojnacki, D., Heath, L., & Birdsey, R. (2003). National-scale biomass estimators for United States tree species. *Forest Science*, 49, 12–35.
- Ji, L., & Gallo, K. (2006). An agreement coefficient for image comparison. *Photogrammetric Engineering and Remote Sensing*, 72, 823–833.
- Kauth, R. J., & Thomas, G. (1976). The tasseled cap—a graphic description of the spectral-temporal development of agricultural crops as seen by Landsat. *LARS Symposia* (pp. 159).
- Kennedy, R. E., Andréfouët, S., Cohen, W. B., Gómez, C., Griffiths, P., Hais, M., ... Zhu, Z. (2014). Bringing an ecological view of change to Landsat-based remote sensing. *Frontiers in Ecology and the Environment*, 12, 339–346.
- Kennedy, R. E., Yang, Z., Braaten, J., Copass, C., Antonova, N., Jordan, C., & Nelson, P. (2015). Attribution of disturbance change agent from Landsat time-series in support of habitat monitoring in the Puget Sound region, USA. *Remote Sensing of Environment*. <http://dx.doi.org/10.1016/j.rse.2015.05.005>.
- Kennedy, R. E., Yang, Z., & Cohen, W. B. (2010). Detecting trends in forest disturbance and recovery using yearly Landsat time series: 1. LandTrendr — Temporal segmentation algorithms. *Remote Sensing of Environment*, 114, 2897–2910.
- Keogh, E., Chu, S., Hart, D., & Pazzani, M. (2001). An online algorithm for segmenting time series. *Data mining, 2001. ICDM 2001, Proceedings IEEE International Conference on* (pp. 289–296).
- Key, C. H., & Benson, N. C. (2006). Landscape assessment. FIREMON: Fire effects monitoring and inventory system. *Gen. Tech. Rep. RMRS-GTR-164-CD, Fort Collins, CO: US Department of Agriculture, Forest Service, Rocky Mountain Research Station*.
- Kurz, W. A., & Apps, M. J. (1999). A 70-year retrospective analysis of carbon fluxes in the Canadian forest sector. *Ecological Applications*, 9, 526–547.
- Lacerte, V., Larocque, G. R., Woods, M., Parton, W. J., & Penner, M. (2006). Calibration of the forest vegetation simulator (FVS) model for the main forest species of Ontario, Canada. *Ecological Modelling*, 199, 336–349.
- Lambert, M.-C., Ung, C.-H., & Raulier, F. (2005). Canadian national tree aboveground biomass equations. *Canadian Journal of Forest Research*, 35, 1996–2018.
- Lefsky, M. A. (2010). A global forest canopy height map from the moderate resolution imaging spectroradiometer and the geoscience laser altimeter system. *Geophysical Research Letters*, 37. <http://dx.doi.org/10.1029/2010GL043622>.
- Lefsky, M. A., Cohen, W. B., Parker, G. G., & Harding, D. J. (2002). Lidar remote sensing for ecosystem studies. *Bioscience*, 52, 19–30.
- Lessard, V. C., McRoberts, R. E., & Holdaway, M. R. (2001). Diameter growth models using Minnesota forest inventory and analysis data. *Forest Science*, 47, 301–310.
- Li, Y., Andersen, H. -E., & McGaughey, R. (2008). A comparison of statistical methods for estimating forest biomass from light detection and ranging data. *Western Journal of Applied Forestry*, 23, 223–231.
- Lu, D. (2006). The potential and challenge of remote sensing-based biomass estimation. *International Journal of Remote Sensing*, 27, 1297–1328.
- Magnussen, S., & Russo, G. (2012). Uncertainty in photo-interpreted forest inventory variables and effects on estimates of error in Canada's National Forest Inventory. *The Forestry Chronicle*, 88, 439–447.
- Main-Knorn, M., Cohen, W. B., Kennedy, R. E., Grodzki, W., Pflugmacher, D., Griffiths, P., & Hostert, P. (2013). Monitoring coniferous forest biomass change using a Landsat trajectory-based approach. *Remote Sensing of Environment*, 139, 277–290.
- Masek, J. G., Huang, C., Wolfe, R., Cohen, W., Hall, F., Kutler, J., & Nelson, P. (2008). North American forest disturbance mapped from a decadal Landsat record. *Remote Sensing of Environment*, 112, 2914–2926.
- McGaughey, R. (2013). *FUSION/LDV: Software for LIDAR data analysis and visualization*. Seattle, WA, USA: US Department of Agriculture, Forest Service, Pacific Northwest Research Station.
- McRoberts, R. E., & Tomppo, E. O. (2007). Remote sensing support for national forest inventories. *Remote Sensing of Environment*, 110, 412–419.
- McRoberts, R. E., Tomppo, E. O., Finley, A. O., & Heikkinen, J. (2007). Estimating areal means and variances of forest attributes using the k-nearest neighbors technique and satellite imagery. *Remote Sensing of Environment*, 111, 466–480.
- Millennium Ecosystem Assessment (2005). *Ecosystems and human well-being: Synthesis*. Washington, DC: Island Press.
- Miller, J. D., Knapp, E. E., Key, C. H., Skinner, C. N., Isbell, C. J., Creasy, R. M., & Sherlock, J. W. (2009). Calibration and validation of the relative differentiated Normalized Burn Ratio (RdNBR) to three measures of fire severity in the Sierra Nevada and Klamath Mountains, California, USA. *Remote Sensing of Environment*, 113(3), 645–656.
- Moer, M., & Stage, A. R. (1995). Most similar neighbor: An improved sampling inference procedure for natural resource planning. *Forest Science*, 41, 337–359.
- Moer, M., Ohmann, J. L., Kennedy, R. E., Cohen, W. B., Yang, Z., Gregory, M. J., ... Fiorella, M. (2011). Northwest forest plan — Status and trends of late-successional and old-growth forests from 1994 to 2008. PNW-GTR-853, Pacific Northwest Research Station, USDA Forest Service, Portland, OR.
- Natural Resources Canada (1995). *National Topographic Database*. ON: Ottawa.
- Natural Resources Canada (2014). *The state of Canada's forests. Annual Report*. Ottawa, ON: Natural Resources Canada, Canadian Forest Service (Accessed online on May 29th, 2015 at <https://cfs.nrcan.gc.ca/publications/download-pdf/35713>).
- Nielsen, U., Aldred, A. H., & MacLeod, D. A. (1979). A forest inventory in the Yukon using large-scale photo sampling techniques. *Information Report FMR-X-121*. Ottawa, Canada: Canadian Forestry Service, Forest Management Institute.
- Ohmann, J. L., & Gregory, M. J. (2002). Predictive mapping of forest composition and structure with direct gradient analysis and nearest-neighbor imputation in coastal Oregon, USA. *Canadian Journal of Forest Research*, 32, 725–741.
- Ohmann, J. L., Gregory, M. J., Roberts, H. M., Cohen, W. B., Kennedy, R. E., & Yang, Z. (2012). Mapping change of older forest with nearest-neighbor imputation and Landsat time-series. *Forest Ecology and Management*, 272, 13–25.
- Pflugmacher, D., Cohen, W. B., & Kennedy, R. E. (2012). Using Landsat-derived disturbance history (1972–2010) to predict current forest structure. *Remote Sensing of Environment*, 122, 146–165.
- Pflugmacher, D., Cohen, W. B., Kennedy, R. E., & Yang, Z. (2014). Using Landsat-derived disturbance and recovery history and lidar to map forest biomass dynamics. *Remote Sensing of Environment*, 151, 124–137.
- Pierce, K. B., Ohmann, J. L., Wimberly, M. C., Grgeory, M. J., & Fried, J. S. (2009). Mapping wildland fuels and forest structure for land management: a comparison of nearest neighbor imputation and other methods. *Canadian Journal of Forest Research*, 39, 1901–1916.
- Poso, S. (2006). Change monitoring with permanent sample plots. *Forest Inventory*. Netherlands: Springer.
- Potapov, P., Turubanova, S., & Hansen, M. C. (2011). Regional-scale boreal forest cover and change mapping using Landsat data composites for European Russia. *Remote Sensing of Environment*, 115, 548–561.
- Powell, S. L., Cohen, W. B., Healey, S. P., Kennedy, R. E., Moisen, G. G., Pierce, K. B., & Ohmann, J. L. (2010). Quantification of live aboveground forest biomass dynamics with Landsat time-series and field inventory data: A comparison of empirical modeling approaches. *Remote Sensing of Environment*, 114, 1053–1068.
- Powell, S. L., Cohen, W. B., Yang, Z., Pierce, J. D., & Alberti, M. (2008). Quantification of impervious surface in the Snohomish water resources inventory area of western Washington from 1972–2006. *Remote Sensing of Environment*, 112, 1895–1908.
- Prasad, A. M., Iverson, L. R., & Liaw, A. (2006). Newer classification and regression tree techniques: Bagging and random forests for ecological prediction. *Ecosystems*, 9, 181–199.
- Reutebuch, S. E., Andersen, H. -E., & McGaughey, R. J. (2005). Light detection and ranging (LIDAR): An emerging tool for multiple resource inventory. *Journal of Forestry*, 103, 286–292.
- Riemann, R., Wilson, B. T., Lister, A., & Parks, S. (2010). An effective assessment protocol for continuous geospatial datasets of forest characteristics using USFS Forest Inventory and Analysis (FIA) data. *Remote Sensing of Environment*, 114, 2337–2352.
- Roberts, D. W., & Cooper, S. V. (1989). Concepts and techniques of vegetation mapping. *Land classifications based on vegetation: Applications for resource management* (pp. 90–96). Ogden, UT: USDA Forest Service GTR INT-257.
- Roy, D. P., Ju, J., Kline, K., Scaramuzza, P. L., Kovalsky, V., Hansen, M., ... Zhang, C. (2010). Web-enabled Landsat data (WELD): Landsat ETM+ composited mosaics of the conterminous United States. *Remote Sensing of Environment*, 114, 35–49.
- Roy, D. P., Wulder, M., Loveland, T., Woodcock, C., Allen, R., Anderson, M., ... Kennedy, R. (2014). Landsat-8: Science and product vision for terrestrial global change research. *Remote Sensing of Environment*, 145, 154–172.
- Russell, R. E., Saab, V. A., Dudley, J. G., & Rotella, J. J. (2006). Snag longevity in relation to wildfire and postfire salvage logging. *Forest Ecology and Management*, 232, 179–187.
- Schmidt, G., Jenkinson, C., Masek, J., Vermote, E., & Gao, F. (2013). Landsat ecosystem disturbance adaptive processing system (LEDAPS) algorithm description. *US Geological Survey Open-File Report*, 1057, 17.
- Simard, M., Pinto, N., Fisher, J. B., & Baccini, A. (2011). Mapping forest canopy height globally with spaceborne lidar. *Journal of Geophysical Research*, 116. <http://dx.doi.org/10.1029/2011JG001708>.
- Smith, S. H., Bell, J. F., Herman, F. R., & See, T. (1984). *Growth and yield of Sitka spruce and western hemlock at Cascade Head experimental forest, Oregon*. Portland, OR: USDA Forest Service RP-PNW-325 (30 pp.).
- Smith, W. B. (2002). Forest inventory and analysis: A national inventory and monitoring program. *Environmental Pollution*, 116, S233–S242.
- Smithwick, E. A. H., Harmon, M. E., Remillard, S. M., Acker, S. A., & Franklin, J. F. (2002). Potential upper bounds of carbon stores in forests of the Pacific northwest. *Ecological Applications*, 12, 1303–1317.
- Ståhl, G., Holm, S., Gregoire, G., Gobakken, T., Næsset, E., & Nelson, R. (2011). Model-based inference for biomass estimation in a LiDAR sample survey in Hedmark County, Norway. *Canadian Journal of Forest Research*, 41, 96–107.

- Stocks, B. J., Mason, J. A., Todd, J. B., Bosch, E. M., Wotton, B. M., Amiro, B. D., ... Skinner, W. R. (2002). Large forest fires in Canada, 1959–1997. *Journal of Geophysical Research: Atmospheres (1984–2012)*, 107(D1), FFR-5.
- Strunk, J. L., Temesgen, H., Andersen, H.-E., & Packalen, P. (2014). Prediction of forest attributes with field plots, Landsat, and a sample of lidar strips. *Photogrammetric Engineering & Remote Sensing*, 80, 143–150.
- Temesgen, H., Affleck, D., Poudel, K., Gray, A., & Sessions, J. (2015). A review of the challenges and opportunities in estimating above ground forest biomass using tree-level models. *Scandinavian Journal of Forestry*, 30, 326–335.
- Tompalski, P., Coops, N. C., White, J. C., & Wulder, M. A. (2014). Simulating the impacts of error in species and height upon tree volume derived from airborne laser scanning data. *Forest Ecology and Management*, 327, 167–177.
- Tomppo, E., Gschwantner, T., Lawrence, M., McRoberts, R. E., Gabler, K., Schadauer, K., ... Cienciala, E. (2010). National Forest Inventories. *Pathways for common reporting* (pp. 541–553). European Science Foundation.
- Tomppo, E., Olsson, H., Ståhl, G., Nilsson, M., Hagner, O., & Katila, M. (2008). Combining national forest inventory field plots and remote sensing data for forest databases. *Remote Sensing of Environment*, 112, 1982–1999.
- Ung, C.-H., Bernier, P., & Guo, X.-J. (2008). Canadian national biomass equations: New parameter estimates that include British Columbia data. *Canadian Journal of Forest Research*, 38, 1123–1132.
- White, J., & Wulder, M. (2013). The Landsat observation record of Canada. *Canadian Journal of Remote Sensing*, 39, 455–467.
- White, J., Wulder, M., Hobart, G., Luther, J., Hermosilla, T., Griffiths, P., ... Dyk, A. (2014). Pixel-based image compositing for large-area dense time series applications and science. *Canadian Journal of Remote Sensing*, 40, 192–212.
- White, J. C., Wulder, M. A., Varhola, A., Vastaranta, M., Coops, N. C., Cook, B. D., ... Woods, M. (2013). A best practices guide for generating forest inventory attributes from airborne laser scanning data using an area-based approach. *Canadian Forest Service, Canadian Wood Fibre Centre, Information Report FI-X-010* (Accessed on November 22, 2015 at <http://www.cfs.nrcan.gc.ca/pubwarehouse/pdfs/34887.pdf>).
- Wickham, H. (2009). *ggplot2: Elegant graphics for data analysis*. (Spring New York).
- Wilson, B. T., Woodall, C. W., & Griffith, D. M. (2013). Imputing forest carbon stock estimates from inventory plots to a nationally continuous coverage. *Carbon Balance and Management*, 8, 1.
- Woodbury, P. B., Smith, J. E., & Heath, L. S. (2007). Carbon sequestration in the US forest sector from 1990 to 2010. *Forest Ecology and Management*, 241, 14–27.
- Woodcock, C. E., Allen, R., Anderson, M., Belward, A., Bindschadler, R., Cohen, W., ... Helmer, E. (2008). Free access to Landsat imagery. *Science*, 320, 1011.
- Woodcock, C. E., Collins, J. B., Gopal, S., Jakabhazy, V. D., Li, X., Macomber, S., ... Wu, Y. (1994). Mapping forest vegetation using Landsat TM imagery and a canopy reflectance model. *Remote Sensing of Environment*, 50, 240–254.
- Wulder, M. A., Masek, J. G., Cohen, W. B., Loveland, T. R., & Woodcock, C. E. (2012a). Opening the archive: How free data has enabled the science and monitoring promise of Landsat. *Remote Sensing of Environment*, 122, 2–10.
- Wulder, M. A., White, J. C., Bater, C. W., Coops, N. C., Hopkinson, C., & Chen, G. (2012b). Lidar plots—A new large-area data collection option: Context, concepts, and case study. *Canadian Journal of Remote Sensing*, 38, 600–618.
- Wulder, M. A., Kurz, W. A., & Gillis, M. (2004). National level forest monitoring and modeling in Canada. *Progress in Planning*, 61, 365–381.
- Wulder, M. A., White, J. C., Cranny, M., Hall, R. J., Luther, J. E., Beaudoin, A., ... Dechka, J. A. (2008). Monitoring Canada's forests. Part 1: Completion of the EOSD land cover project. *Canadian Journal of Remote Sensing*, 34, 549–562.
- Zald, H. S., Ohmann, J. L., Roberts, H. M., Gregory, M. J., Henderson, E. B., McGaughey, R. J., & Braaten, J. (2014). Influence of lidar, Landsat imagery, disturbance history, plot location accuracy, and plot size on accuracy of imputation maps of forest composition and structure. *Remote Sensing of Environment*, 143, 26–38.
- Zhu, Z., & Woodcock, C. E. (2012). Object-based cloud and cloud shadow detection in Landsat imagery. *Remote Sensing of Environment*, 118, 83–94.